Published by IOP Publishing for Sissa Medialab

Received: *May 14, 2025*
Accepted: *June 17, 2025*
Published: *July 16, 2025*

20th Anniversary Trento Workshop on Advanced Silicon Radiation Detectors
Trento, Italy
4–6 February 2025

High-resolution, high-dynamic-range charge detector for ion beam monitoring

O. Adriani[a,b] **E. Berti**[a] **P. Betti**[a] **J. Casaus**[d] **R. D'Alessandro**[a,b] **S. Detti**[a] **C. Diaz**[d] **J. Marin**[d] **G. Martinez**[d] **N. Mori**[a] **L. Pacini**[a] **C. Pizzolotto**[c] **A. Tiberio**[a,b] **M. Scaringella**[a] **O. Starodubtsev**[a,*] **G. Zampa**[c] **and N. Zampa**[c]

[a] *Istituto Nazionale di Fisica Nucleare, Sezione di Firenze, Via Bruno Rossi 3, Sesto Fiorentino, Italy*
[b] *Department of Physics and Astronomy, University of Florence, Via Sansone 1, Sesto Fiorentino, Italy*
[c] *Istituto Nazionale di Fisica Nucleare, Sezione di Trieste, Via A. Valerio 2, Trieste, Italy, I-34149 Trieste, Italy*
[d] *Centro de Investigaciones Energéticas, Medioambientales y Tecnológicas (CIEMAT), Avenida Complutense 40, Madrid, Spain*

E-mail: starodubtsev@fi.infn.it

Abstract: We present the second-generation charge detector, designed to further improve resolution, dynamic range, and robustness for high-energy ion beam monitoring. This upgraded prototype incorporates enhanced silicon photodiodes, a refined front-end electronics design, and optimized mechanical construction to improve noise performance and operational stability. Extensive testing during HERD and AMS beam campaigns at CERN SPS demonstrated significant performance gains over the first version, achieving superior charge resolution and maintaining a dynamic range capable of accurately measuring nuclei from Z = 1 up to Z ≈ 80. The detector's fast, real-time data analysis capabilities have also been strengthened, confirming its suitability for online monitoring applications. In this article, we summarize the new developments, present updated test results, and outline future improvements, including adaptations for broader applications in beam monitoring, nuclear cross-section measurements, and cosmic-ray studies.

Keywords: Heavy-ion detectors; Instrumentation and methods for heavy-ion reactions and fission studies; Ion identification systems; Particle identification methods

*Corresponding author.

https://doi.org/10.1088/1748-0221/20/07/C07046

Contents

1 Introduction

The device presented in this article is a next-generation charge tagger [1]. This study was initiated within the framework of the HERD collaboration by the INFN Florence team, in partnership with INFN Trieste and CIEMAT (Madrid, Spain). The High Energy cosmic-Radiation Detection (HERD) facility is slated to operate aboard the Chinese Space Station (CSS) starting around 2027, with a planned mission duration of approximately ten years. HERD's scientific goals target several frontier research areas, including the indirect detection of dark matter with unprecedented sensitivity, high-precision measurements of cosmic ray spectra and composition up to the knee region, and comprehensive gamma-ray sky monitoring [2].

The HERD instrument features a central 3D-segmented, deep, homogeneous calorimeter, surrounded by a suite of subsystems including scintillating fiber trackers, anti-coincidence detectors, silicon-based charge detectors, and a transition radiation detector [3]. The detector design maximizes geometric acceptance and pushes the measurement capability well beyond current direct-detection experiments, potentially reaching PeV energies for light nuclei. This project aims to enhance our understanding of cosmic ray acceleration and propagation mechanisms within the Galaxy, by enabling detailed measurements of proton and nuclei fluxes beyond hundreds of TeV per nucleon. Furthermore, HERD will investigate electron spectra in the multi-TeV range, offering an opportunity to identify potential dark matter signals or pinpoint nearby astrophysical sources. Thanks to its wide field of view, HERD will also serve as a powerful instrument for gamma-ray sky surveys in the energy window spanning from a few hundred MeV up to 1 TeV.

During the R&D phase, HERD's subsystems and components were subjected to comprehensive testing campaigns at various facilities, including CERN's Proton Synchrotron (PS) and Super Proton Synchrotron (SPS) [4], as well as other beamlines [5, 6]. Testing with heavy ion beams at SPS revealed the urgent need for accurate and reliable beam quality monitoring. Although HERD includes a built-in charge detector, its current dynamic range is limited to around Z~26, and it utilizes silicon microstrip sensors that require complex calibration and lengthy data analysis procedures [7]. These limitations render it impractical for real-time monitoring purposes. To overcome this, we have developed a real-time, user-friendly, and cost-effective charge tagging solution tailored for beam diagnostics.

2 Detector design

The charge tagger operates based on the principle of direct ionization occurring in the depleted region of silicon photodiodes.

For first design [1], we reused photodiodes originally developed for the CaloCube R&D project [8], which had validated the 3D calorimetric concept later adopted in HERD. This prototype consisted of six blinded photodiodes arranged in a linear array (figure 1). The design emphasized simplicity and low mass, employing a custom-built, lightweight mechanical structure that allowed quick installation and removal. The structure's reduced material budget helped limit fragmentation of incoming nuclei within the detector.

To streamline development and ensure compatibility, the prototype employed the same front-end electronics as the HERD calorimeter photodiode system [9]. This approach provided a wide dynamic range, low noise performance, and straightforward integration with existing trigger and data acquisition systems, demonstrating the charge tagger's potential for real-time applications within HERD.

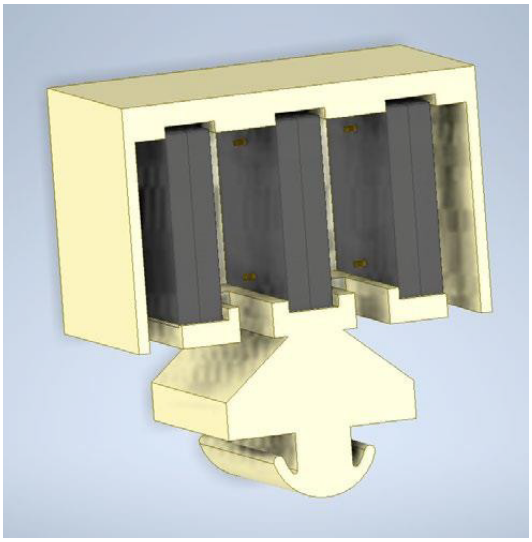

Figure 1. First prototype mechanical design. 6 blinded PDs in their package (the black elements in the figure) are mounted in 3 pairs.

Despite demonstrating good performance, the initial prototype exhibited several limitations that impacted its overall efficiency and suitability for broader applications:

- Limited active area: each photodiode had an active area of only 9.8×9.8 mm^2, restricting spatial coverage and requiring precise alignment.
- Challenging mechanical alignment: the one-dimensional linear configuration, combined with the mechanical frame, made accurate alignment along the beamline more difficult and time-consuming.
- High passive material budget: each photodiode package contributed approximately 1.5 mm of passive material, leading to a cumulative total of about 12 mm across the entire detector. This substantial amount of passive material increased the probability of nuclear fragmentation before the charge measurement could occur, affecting the accuracy of charge identification.

2025 JINST 20 C07046

- Component obsolescence: the specific model of photodiodes used in the first prototype is no longer in production, posing challenges for scalability and long-term maintenance.

- Suboptimal electrical connection: the mechanical and electrical interface between the photodiodes and the front-end electronics was not ideal, leading to potential issues with signal integrity and noise performance.

These limitations underscored the need for a more robust, scalable, and high-performance solution. In response, a second-generation prototype was developed with a strong emphasis on improving geometrical efficiency, mechanical stability, and signal integrity. By addressing the constraints identified in the initial version, particularly in terms of active area coverage, material budget, and electronic interfacing, the new design incorporates significant upgrades. These include larger, unpackaged photodiodes arranged in modular 3×3 matrices, a custom low-noise PCB for optimized readout, and a mechanically simplified structure to streamline assembly and alignment. Together, these enhancements aim to significantly improve the detector's performance, reliability, and applicability in high-energy beam monitoring environments.

Building on the experience and results from the initial prototype, a second, more advanced charge tagger was developed. This version aimed to overcome the previously identified limitations while maintaining simplicity, robustness, and compatibility with the HERD test infrastructure.

The new prototype adopts a modular 3×3 matrix configuration, with each module comprising nine unpackaged silicon photodiodes featuring a 10×10 mm^2 active area. The removal of the photodiode packaging significantly reduces the passive material budget along the beamline.

A custom-designed printed circuit board (PCB) was developed to support the photodiodes mechanically and electrically. The PCB layout was optimized for low noise, individual biasing, and robust signal routing, ensuring high signal fidelity and improved overall detector performance. Coaxial cable connections are used to preserve signal integrity, and dedicated bias lines allow precise control and monitoring of each diode's operating conditions. Figure 2 illustrates the new PCB design.

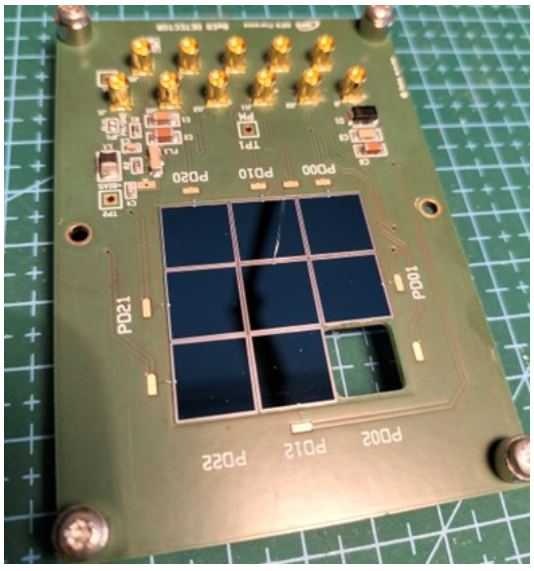

Figure 2. Updated Mechanical Design — Ongoing Installation of 3×3 Matrix Photodetectors (PDs).

2025 JINST 20 C07046

This modular design approach offers several advantages:

- Scalability and flexibility: the detector can be easily adapted for different beamline geometries or particle species.
- Simplified integration and maintenance: the plug-and-play nature of the modules facilitates rapid installation, testing, and replacement.

In addition to improved mechanical and electrical performance, the second prototype maintains full compatibility with the HERD front-end readout electronics and data acquisition systems. This ensures that it remains a practical and deployable solution for both beam monitoring and charge tagging in future test campaigns and potential permanent installations.

2.1 Diode

To address the limitations identified in the first prototype, including limited active area, high passive material budget due to packaged components, and complex mechanical integration, we developed a second-generation detector based on a new photodiode type: the VTH2120 by Excelitas [10].

The VTH2120 is a large-area ($10 \times 10\,\mathrm{mm}^2$) silicon photodiode provided in chip form without any external package or window. This package-free configuration significantly reduces the passive material along the beamline, thereby minimizing unwanted nuclear fragmentation and improving charge resolution. The diode is optimized for direct ionization detection in high-energy particle experiments. Its high breakdown voltage allows the application of large reverse bias, enabling full depletion of the diode volume. Combined with a relatively large depletion thickness of approximately 250 µm, the device ensures high signal yield and fast charge collection, thanks to the strong internal electric field. This configuration provides uniform response across different diodes, supporting precise charge measurement and reliable detector performance.

Key characteristics of the VTH2120 include:

- Active area: $10{\times}10\,\mathrm{mm}^2$, offering a 30% increase in sensitive surface compared to the previous prototype.
- Dark current: <5 nA at 20 V reverse bias, which ensures low intrinsic noise.
- Capacitance: <120 pF, supporting high signal fidelity and fast response.
- Low-profile design, suitable for environments with limited spatial allowance.
- Backside metallization, allowing electrical contact via conductive epoxy, which simplifies integration with the custom PCB.

Before assembly into the detector matrix, all photodiodes (PDs) underwent a comprehensive characterization campaign to ensure consistent performance and optimal selection. This step was critical to guarantee uniform detector response, minimize noise, and optimize the biasing conditions. The following electrical and physical parameters were measured:

- Current-Voltage (I-V) curves: each photodiode was tested for leakage current under reverse bias conditions. Only devices exhibiting low leakage current, typically in the nanoampere range, were selected for use to maintain a high signal-to-noise ratio. Figure 3 illustrates the leakage current distribution at 180 V reverse bias.

2025 JINST 20 C07046

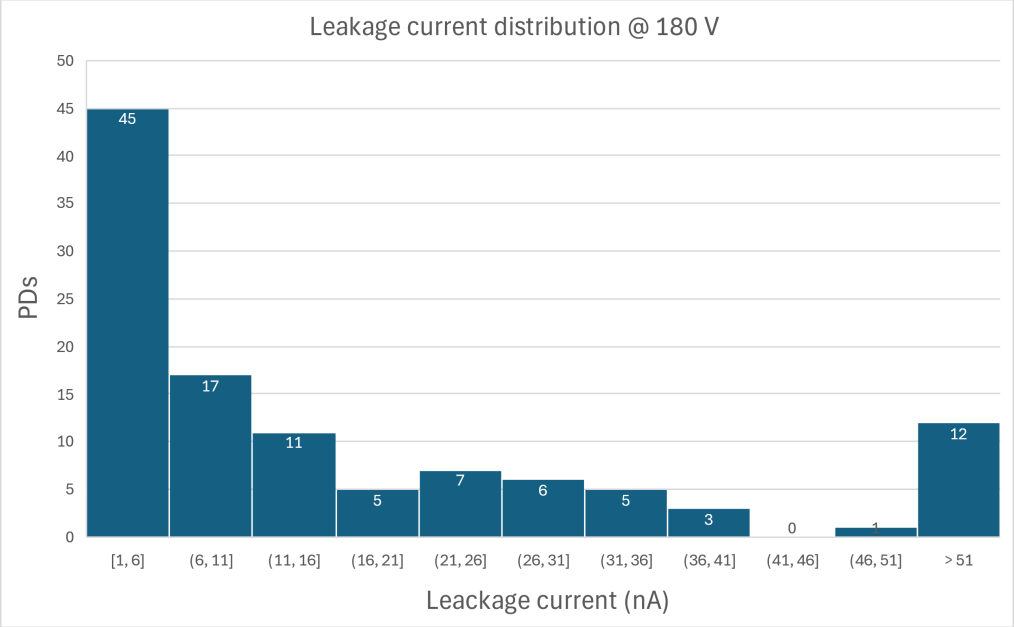

Figure 3. Leakage current distribution at 180 V reverse bias.

- Breakdown voltage: the maximum reverse bias voltage the diode can sustain without entering avalanche breakdown was measured. Devices with sufficiently high breakdown voltages (>140 V) were preferred to ensure safe operation under varying beam conditions.
- Capacitance-Voltage (C-V) analysis (performed on a subset of diodes): this test allowed extraction of key parameters such as the full depletion voltage, which defines the operating point where the depletion region spans the entire active thickness of the device. Operating above this voltage ensures full charge collection.
- Depletion depth estimation: derived from the C-V measurements and/or manufacturer specifications, the depletion depth determines the detector's active thickness and thus its charge collection efficiency for minimum ionizing particles or heavy ions.

Figure 4 (top) presents an example of I-V characteristics, while figure 4 (bottom) illustrates C-V measurements.

This photodiode was integrated into a 3×3 matrix configuration, enabling scalable modular architecture and improved spatial granularity. These tests allowed grouping of photodiodes with similar characteristics to ensure uniform response across the 3×3 matrix, improve matching with the front-end electronics, and minimize calibration complexity. Uniformity in breakdown voltage was critical to streamline the high-voltage biasing scheme using shared supply lines.

This level of pre-selection and testing improves not only the performance but also the reliability and long-term stability of the detector, especially in environments with limited access or where real-time monitoring is essential.

The mechanical support and electronics layout were redesigned accordingly to match the flat chip geometry, improve noise performance, and streamline the assembly. The use of coaxial cabling and dedicated bias lines further enhances signal integrity and operational stability.

2025 JINST 20 C07046

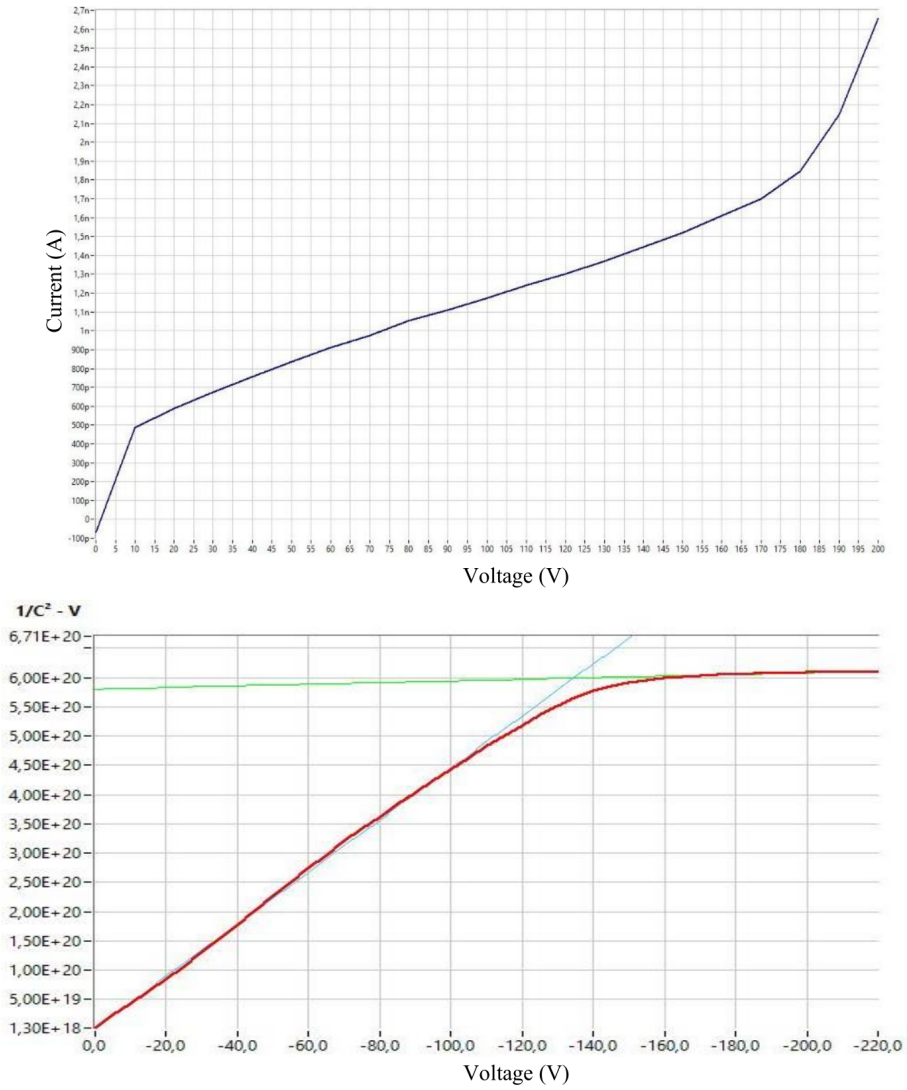

Figure 4. Top: example of I-V characteristics. Bottom: C-V characteristic of the photodiode. The lines indicate two fits which cross-section corresponds to the depletion voltage.

The new sensor and layout approach represent a major step forward in performance, manufacturability, and adaptability for beam monitoring and charge tagging applications in high-energy ion beams.

2.2 Electronics

The second version of charge tagger employs the HiDRA version 2 ASIC, a low-noise, low-power front-end chip developed by INFN Trieste for spaceborne calorimetric applications. This is the same chip used for the firs charge tagger version [1] and HERD experiment [11]. HiDRA v2 is an evolution of the CASIS chip and was selected for its high dynamic range and proven compatibility with silicon photodiodes such as the VTH2120.

Key features of the HiDRA v2 include:

- Dual-gain charge-sensitive amplifier (CSA) with automatic gain switching (dynamic range from a few femtocoulombs up to ~52 pC)

2025 JINST 20 C07046

- Low noise (ENC ≈ 2500 electrons) and low power consumption (~3.75 mW/channel)
- 16 channels per chip with analog multiplexed output
- Self-trigger capability, with four selectable threshold levels
- Acquisition rate up to 1 kHz

Each CSA output is processed through a correlated double sampling (CDS) circuit and a fast trigger chain, enabling accurate signal reconstruction and real-time event selection. The gain-switching mechanism is highly stable, with a transition uncertainty below 1%. Trigger signals from adjacent channels are ORed and converted to differential CMOS format to reduce output complexity.

Figure 5 (left) illustrates the block scheme of a single channel of a HiDRA 2 ASIC, while figure 5 (right) shows one front-end board containing four chips.

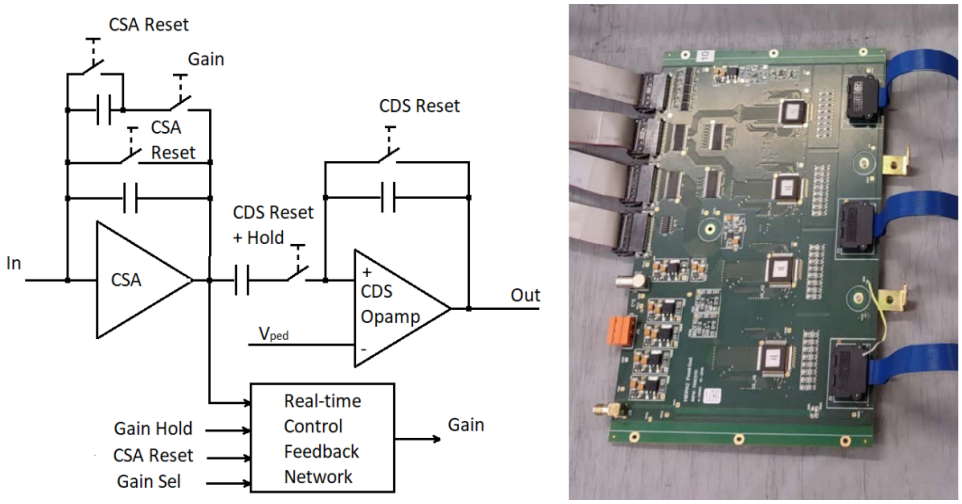

Figure 5. Left: the block scheme of a single channel of a HiDRA 2. Right: HERD calorimeter front-end board containing four chips.

To complement the upgraded photodiode array and the high-performance HiDRA v2 readout ASIC, discussed above custom PCB fulfills several critical functions:

- Mechanical support and precise alignment of the photodiode matrix, ensuring stability and repeatability in the beam environment.
- Minimization of electrical noise, achieved through passive bias filters, careful layout design, short signal paths, and controlled impedance traces.
- Use of coaxial cables with MCA connectors for all analog connections between the photodiodes and front-end electronics, which significantly reduces external interference, crosstalk and mechanical stability.
- Dedicated high-voltage bias lines routed to each photodiode group, allowing for independent bias control and better performance tuning across the array.

2025 JINST 20 C07046

This integrated design ensures compatibility with the HiDRA v2 front-end boards while maintaining low material budget along the beam path. The combined system comprising unpackaged photodiodes, a modular mechanical frame, custom PCBs, and low-noise readout electronics offers excellent scalability, improved signal fidelity, and robust performance, making it well-suited for both laboratory testing and beamline deployment in high-energy physics experiments.

2.3 Prototypes

As part of the development process, two complete detector units were built, each consisting of six identical modules, with each module housing a 3×3 matrix of photodiodes (PDs), a total of 54 PDs per detector (figure 6). The photodiodes were carefully tested, selected, and grouped based on critical electrical parameters, including leakage current, breakdown voltage, and depletion characteristics, to ensure optimal and uniform performance across each module.

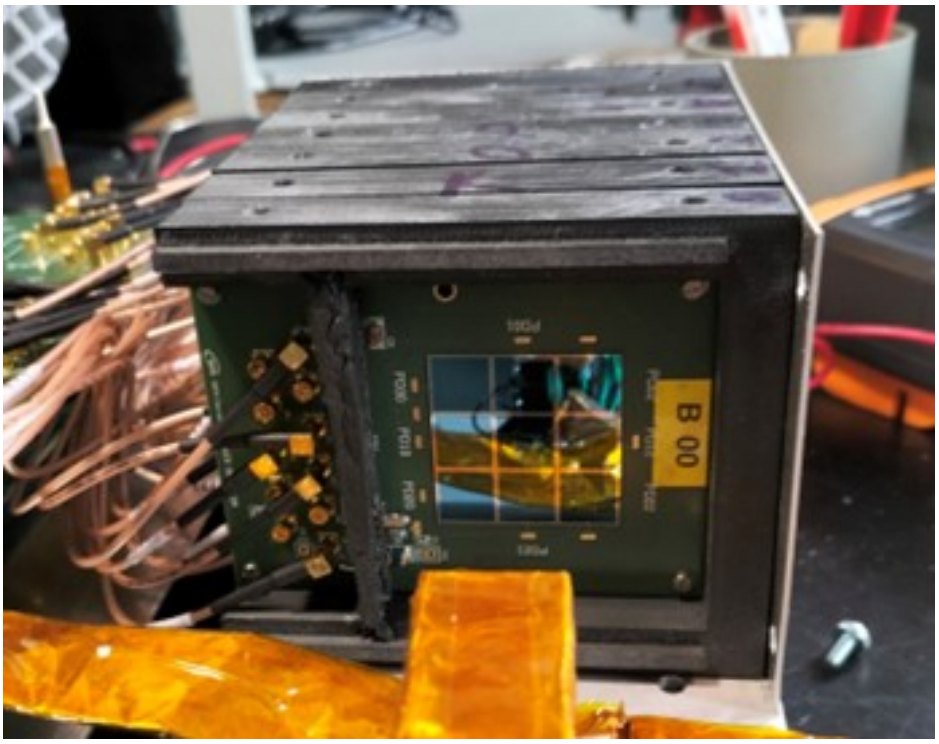

Figure 6. Second generation charge tagger.

As was mentioned above, in some cases, additional capacitance-voltage (C-V) measurements were carried out to evaluate full depletion voltage and depletion depth, further enhancing the consistency and predictability of the detector response. This comprehensive selection and grouping strategy were integrated with a modular mechanical design and custom electronics optimized for low-noise operation and reliable connectivity.

3 Data analysis routine

Due to the updated detector design, the data analysis routine had to be revised to accommodate the new configuration. For each horizontal line, comprising six photodiodes (PDs) arranged in a row, the

2025 JINST 20 C07046

following steps are applied, following an approach similar to that used for the first prototype [1]:

- Signal amplitude evaluation: the signal from each of the six PDs is measured in ADC counts and must exceed three times the noise threshold to be considered valid.
- ADC-to-MIP conversion: signals are then converted from ADC units to Minimum Ionizing Particle (MIP) units using calibration parameters specific to each diode. These conversion factors are obtained by analyzing the carbon peak in the fragmented SPS ion beam.
- MIP-to-Z conversion: the signal in MIP units is further converted to the corresponding atomic number (Z).
- Consistency check: only events in which all six PDs produce consistent signals, i.e., differing by less than 1.5 charge units, are accepted for further analysis.

Once the procedure is completed for each row, the best-performing line is selected as the one with the highest reconstructed charge. The analysis software also stores additional information, such as the reconstructed charges for all nine possible lines in each detector, enabling users to perform more advanced and detailed analyses beyond the default reconstruction strategy.

4 Test results

In 2024, the second version of the charge tagger was tested at the SPS facility at CERN using high-energy ion beams. The detector was employed by the HERD collaboration to support performance studies of a large-scale HERD prototype under irradiation with heavy nuclei. The ion beam was produced by directing a 150 GeV/nucleon primary lead beam onto a 4 cm thick beryllium target. The resulting secondary beam, composed of nuclear fragments, was momentum- and rigidity-selected using magnetic optics, allowing for the selection of specific mass-to-charge (A/Z) ratios. This procedure enabled the delivery of ion species spanning a broad range of atomic numbers, from Z = 1 to Z = 82 [12]. By tuning the A/Z values, the composition of the fragmented beam could be tailored to target different elements.

he beam intensity, approximately 1 kHz, was close to the acquisition rate limit of our system. However, this choice ensured the collection of maximal statistics while maintaining an acceptable level of pile-up effects.

The first version of the charge tagger had previously been used during AMS-02 beam tests, where it provided an independent beam monitoring system and supported the characterization of silicon microstrip detectors. Following its application, the AMS-02 collaboration expressed interest in utilizing the updated version of the detector.

The careful selection and characterization of photodiodes (PDs) allowed for grouping of devices with consistent electrical properties. This facilitated the application of a uniform and optimal operating voltage across the detector. Combined with dedicated noise reduction strategies such as the use of coaxial cabling, custom PCBs for shielding, and dedicated bias lines as well as refined data analysis routines, these efforts have collectively resulted in a marked enhancement of the detector's overall performance. These optimizations have improved charge resolution, increased signal-to-noise ratio, and ensured greater stability and reliability in beam test environments.

2025 JINST 20 C07046

Figure 7 illustrates the truncated mean charge distribution measured for an ion beam with an A/Z ratio of approximately 2.2. The measured beam composition, shown as a blue histogram, features distinct peaks corresponding to nuclear charges ranging from Z = 1 up to Z = 70. A Gaussian fit was applied to each peak (red curves), with yellow bands indicating the 1-sigma confidence intervals, absent in cases where fits failed. This fitting procedure enables accurate identification of nuclear charge values, confirming the charge tagger's capability to resolve and quantify a broad spectrum of ion species.

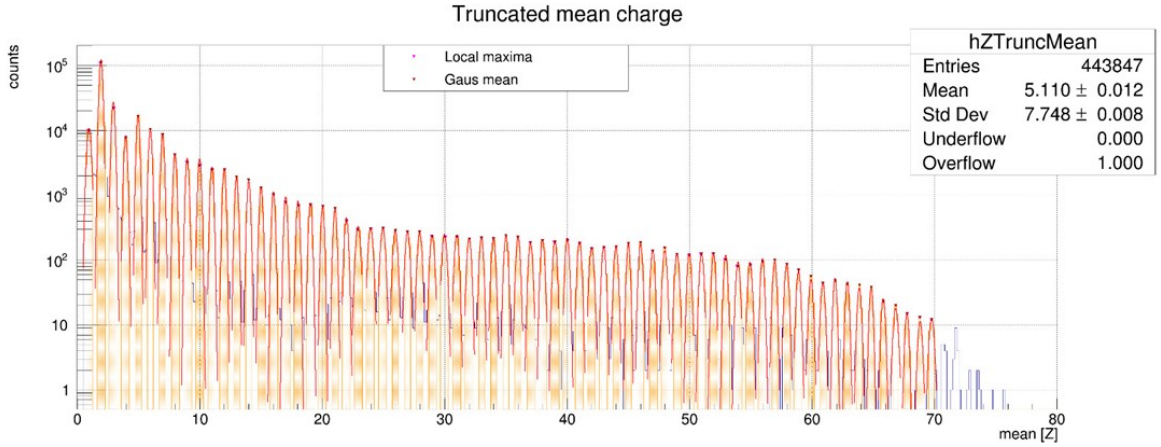

Figure 7. Second generation prototype. Truncated mean charge distribution measured for an ion beam with $A/Z \sim 2.2$.

Figure 8 presents the charge resolution (top panel) and linearity (bottom panel) achieved with the second-generation prototype. Compared to the earlier version, the charge resolution was significantly improved, reaching approximately 0.18 charge units for nuclei up to Z = 70. A deterioration in charge resolution is observed around Z ≈ 24. This effect is likely due to the automatic gain switching feature of the HiDRA front-end chip. While this mechanism effectively extends the system's dynamic range, it can introduce minor nonlinearities or discontinuities near the switching threshold, which may degrade the resolution in this region.

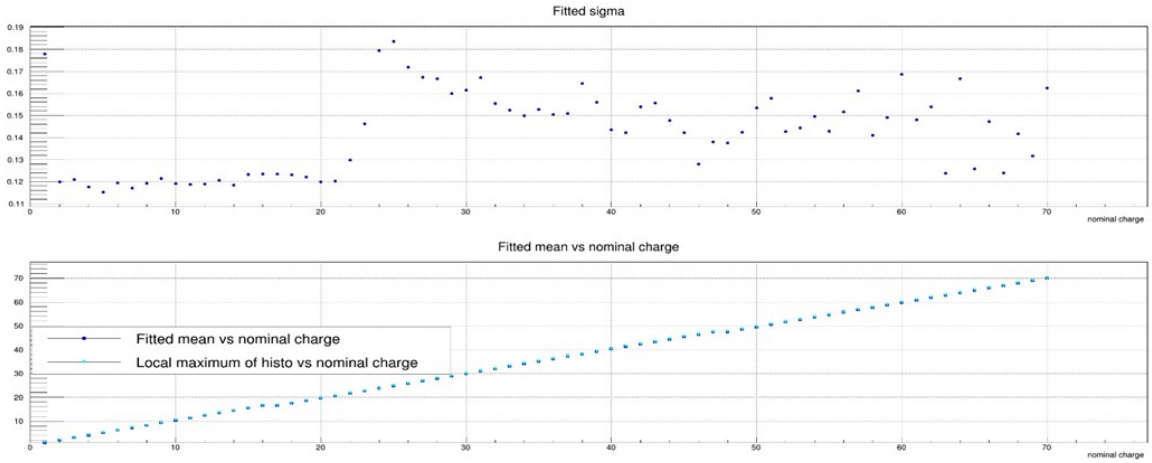

Figure 8. Second generation prototype. Measured resolution and linearity for an ion beam with $A/Z \sim 2.2$.

2025 JINST 20 C07046

Charge linearity was evaluated using two approaches: the local maxima of the measured charge distribution peaks and the mean values obtained from Gaussian fits. In both cases, the detector demonstrated excellent linearity across the full charge range, confirming the robustness and precision of the upgraded system.

To investigate beam fragmentation processes, a dedicated test was conducted employing two charge tagger detectors arranged in a sequential configuration. A block of passive material was strategically placed between the two detectors to induce nuclear fragmentation of the incoming high-energy ions. By correlating the charge measurements from the upstream and downstream detectors, it was possible to identify changes in nuclear charge resulting from interactions with the intermediate material. This setup allowed for a detailed study of fragmentation products and charge-changing processes, offering valuable insight into ion-matter interactions under controlled beam conditions.

Figure 9 presents a two-dimensional correlation plot between the charge values measured by the first and second charge tagger detectors in the beam fragmentation setup. Each axis corresponds to the truncated mean charge measurement from one of the detectors. The clear diagonal trend indicates events in which the nuclear charge remains unchanged, corresponding to unfragmented primary nuclei passing through the intermediate material.

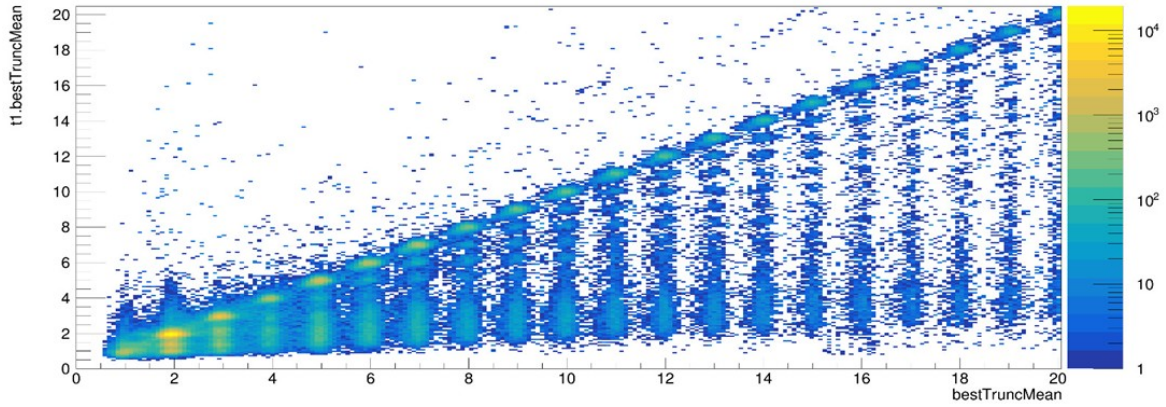

Figure 9. Two-dimensional correlation plot between the charge values measured by the first and second charge tagger detectors.

Beneath each primary peak, distinct vertical structures are observed, representing the charge distributions of secondary nuclei resulting from fragmentation processes. These fragmented nuclei form characteristic families that originate from a given primary nucleus and span a wide range of lower Z values. This pattern reflects the partial or complete stripping of nucleons due to interactions with the passive material placed between the detectors. The events observed above the diagonal are attributed to the pile-up effect, which occurs when the particle rate approaches the upper limit of the detector's acquisition capability.

By analyzing the fraction of fragmented nuclei with respect to the primary beam, one can quantitatively estimate the total and partial nuclear fragmentation cross-sections for various target materials and ion species. The precise charge resolution and redundancy offered by the dual-detector setup enable reliable reconstruction of such cross-sections, supporting detailed studies of nuclear interactions in high-energy ion beams.

2025 JINST 20 C07046

5 Conclusions

These preliminary results demonstrate the promising capabilities of the second-generation charge tagger for high-resolution nuclear charge identification in ion beam environments. The system has proven effective in independently resolving a wide range of nuclei, from Z = 1 up to Z = 60, with a charge resolution of approximately 0.18 charge units. The correlation analysis between two detectors, supported by passive material to induce fragmentation, has clearly shown the emergence of secondary nuclear species under each primary beam component. This ability to resolve and identify fragmentation products offers a powerful method for studying beam composition and nuclear interaction processes.

Moreover, the detector has shown excellent linearity and stability in a challenging beam test environment, confirming the robustness of the selected photodiodes, front-end electronics, and mechanical integration strategy. The modular design, low material budget, and tailored calibration routines have contributed significantly to the detector's performance.

Additional datasets collected during the test campaign are currently under detailed analysis. These data are expected to provide deeper insights into the feasibility and precision of nuclear fragmentation cross-section measurements. The use of dual-detector correlations, combined with known passive material characteristics, holds the potential for quantitative determination of partial and total charge-changing cross-sections. Such capability would represent a significant advancement for beam monitoring, detector calibration, and cosmic ray interaction studies, paving the way for integration of this technology in future space-based and accelerator experiments.

References

[1] O. Adriani et al., *Development of a high-resolution, high-dynamic-range charge detector for ion beam monitoring*, 2025 *JINST* **20** P01019 [arXiv:2412.13934].

[2] A.E. Berti, N. Mori, L. Pacini and O. Starodubtsev, *The High Energy cosmic-Radiation Detection HERD facility: a future space instrument for cosmic-ray detection and gamma-ray astronomy*, *PoS* **ECRS** (2023) 146.

[3] N. Mori and L. Pacini, *The High Energy Cosmic-Radiation Detection (HERD) facility for direct cosmic-ray measurements*, *PoS* **ICHEP2022** (2022) 123.

[4] https://home.cern/news/news/accelerators/accelerator-report-getting-lead-ions-ready-physics.

[5] P. Betti et al., *Photodiode Read-Out System for the Calorimeter of the Herd Experiment*, *Instruments* **6** (2022) 33.

[6] Y. Dong et al., *Experimental verification of the HERD prototype at CERN SPS*, *Proc. SPIE Int. Soc. Opt. Eng.* **9905** (2016) 99056D.

[7] W.-S. Zhang et al., *A novel charge reconstruction algorithm applied to the HERD prototype silicon charge detector*, *Nucl. Instrum. Meth. A* **1064** (2024) 169346.

[8] O. Adriani et al., *The CALOCUBE project for a space based cosmic ray experiment: design, construction, and first performance of a high granularity calorimeter prototype*, 2019 *JINST* **14** P11004 [arXiv:1910.09784].

[9] O. Adriani et al., *Development of the photo-diode subsystem for the HERD calorimeter double-readout*, 2022 *JINST* **17** P09002 [arXiv:2208.04133].

[10] https://www.excelitas.com/file-download/download/public/94706?filename=VTH2120_-_Si_PD__Chip_Form_Series_Datasheet.pdf.

2025 JINST 20 C07046

[11] L. Pacini et al., *Design and expected performances of the large acceptance calorimeter for the HERD space mission*, *PoS* **ICRC2021** (2021) 066.

[12] A. Oliva et al., *The Silicon Charge Detector of the High Energy Cosmic Radiation Detection facility*, *PoS* **ICRC2023** (2023) 087.

2025 JINST 20 C07046